



Modeling of a passive scalar transport from thermal power plants to atmospheric boundary layer

A. A. Issakhov^{1,2} · A. R. Baitureyeva¹

Received: 16 May 2018 / Revised: 26 January 2019 / Accepted: 13 February 2019 / Published online: 21 February 2019
© Islamic Azad University (IAU) 2019

Abstract

At the moment, there is a tendency to increasing the number of thermal power plants (TPPs); this trend can be associated with industrial development and energy consumption growth. This paper discusses the numerical simulation of the pollution movement from activities of the TPP and the study of the pollution concentration level at various distances from the emission source in actual atmospheric conditions. The approbation of the numerical algorithm and the mathematical model was performed using 2D and 3D test problems. The obtained computational values were compared with measured values and computational values of other authors. In addition, the distribution of pollution in the 3D case was investigated on an actual physical size. The Ekibastuz TPP-1 coal-fired power plant was taken as a real example. A distinctive feature of this TPP is that pollution is emitted from two chimneys of different heights ($H_H = 330$ and $H_L = 300$ m). The obtained values illustrated that, due to the difference between the height of the chimney ($H_H - H_L = 30$ m), the pollution concentration from the higher chimney ($H_H = 330$ m) was fell down far away from the emission source than from the lower chimney ($H_L = 300$ m) (2160 and 1970 m, respectively). From the obtained data from computation, it can be argued that the construction of higher chimneys reduces the harmful effects of emissions on the environment. Also, the obtained results will help to predict the optimal and safe distance from cities or settlements during the construction of new thermal power plants.

Keywords Navier–Stokes equations · Thermal power plant · Dispersion · Pollution

Introduction

Air pollution from year to year is becoming a large-scale and serious issue of global significance. Continuous development and population growth in urban areas and many problems related to the environment, such as deforestation, toxic materials emission, solid waste emissions and air pollution attract more attention than ever before. The industry develops all over the world, resulting in a growing number of factories, thermal power plants, nuclear power plants, which produce large amounts of pollutants. Emissions lead to different environmental problems, which are harmful to

the environment and the human health. The air pollution problem in cities has become so serious that there is a need for immediate information about changes in the contamination level (WHO 2002).

Each year, millions of tons of gaseous sulfur oxides and nitrogen oxides are disposed of into the environment. The share of anthropogenic emissions of these oxides from thermal power plants is 45–65% and 15–45%, respectively (WHO 2002). Further development of the thermal energy is highly dependent on ensuring an acceptable level of power plants' impact on the environment and their safety for the ecology. Moreover, these emissions get into the atmosphere and they are distributed by the air, chemically react and fall in the surrounding ground surfaces in the dry form and liquid precipitation (plants, soil, water, buildings). The ambient pollutants can settle at a distance of 100–1000 km from the source depending on chemical, meteorological and various physical factors (Fay and Rosenzweig 1980). This distance increases mainly in proportion to the velocity of the emission source and depends on density, temperature, wind speed, humidity (Zavila 2012; Kozic 2015; Barbero

Editorial responsibility: Parveen Fatemeh Rupani.

✉ A. A. Issakhov
alibek.issakhov@gmail.com

¹ Al-Farabi Kazakh National University, Almaty, Republic of Kazakhstan

² Kazakh British Technical University, Almaty, Republic of Kazakhstan



et al. 2015). In the whole world, about 63% of all electricity is generated by thermal power plants (El-Sharkawi 2013; Olaguer et al. 2016). During the operation of the TPP, fuel is burned and various polluting substances emit into the atmosphere. Many of these contaminations are toxic and, despite the relatively low concentrations, have a negative impact on nature. Air pollution can have a negative impact on human health, the surrounding climate, flora and fauna. Flora is a group of indigenous plants in an ecosystem of a geographical zone, and fauna is a group of indigenous animals of any geographical zone. Contaminants include carbon, sulfur, nitrogen, as well as aerosols and carcinogens. As a result of organic fuel burning in the TPP, carbon dioxide and water formed the main emission components. In addition to the above contaminations from incomplete fuel combustion, the different dust compositions such as sulfur oxides, nitrogen oxides, fluoride compounds, metal oxides and gaseous products are included. After getting into the atmosphere, they cause significant damage not only to the surrounding biosphere but also to buildings, architectural objects, the municipal economy buildings, transport and the nearby area population. About 50% of the pollution from thermal power plant is sulfur dioxide, 30%—nitrogen oxide, and 25%—fly ash (Abbaspour et al. 2005).

The documents regulating the work of TPP are updated every year, in which the permissible norms of emissions into the air basin and reservoirs and solid particle emissions are prescribed. Nowadays various ways are known to reduce emissions from thermal power plants. For example, to limit sulfur dioxide so-called scrubbers (gas scrubbers) are used, which carry out desulfurization of the exhaust gas from the chimneys and remove up to 95% of sulfur dioxide (US Environmental 2016). Direct combustion process is modified in many countries around the world to limit nitric oxide emissions, thereby reducing the nitric oxide release by 30–50% (Environmental, Health, and Safety Guidelines for Thermal Power Plants 2017). There is also a selective catalytic purification method, which allows reducing the nitric oxide release by 80–90%. The advanced technologies for reducing emissions include the CCS (carbon capture and storage) method. At the heart of its principle lies the trapping the carbon dioxide (CO₂) process, after which it is compressed and deposited into underground layers for storage, without letting it out into the atmosphere. Despite the fact that the above technologies provide an instant reduction in air pollution, it does not guarantee a complete exhaustion of the problem. For capturing the CO₂, it can be done also by other technologies. Broadly, three different types of technologies exist: post-combustion, pre-combustion and oxy-fuel combustion.

The study of this process in the Republic of Kazakhstan is especially important. The Republic of Kazakhstan has large reserves of energy resources (oil, gas, coal, uranium). About 80% of exports are raw materials, and the share of

industrial exports decreases annually. According to statistics, Kazakhstan's energy consists of almost 87% coal, and by 2020, the hard fuel proportion will be about 66% of the total volume in the emission generation (Annual report. SAM-RYK ENERGY 2015). Thus, the energy sector is a most polluter of the air basin of the Republic of Kazakhstan.

The simulation of this process can be carried out in two ways: The first is to use a Gaussian model or use the complete momentum and the continuity equations. The Briggs plume rise equations and Gaussian model are often used for contaminants distribution simulation (Fatehifar et al. 2008; Igbokwe et al. 2016; Tomiyama et al. 2016; Gousseau et al. 2011; Ebrahimi and Jahangirian 2013). However, it does not allow a sufficiently accurate smoke movement nature determination. These models showed a good result only in the flat and linear terrain. As a consequence, it is necessary to use a numerical turbulent model that will allow for taking into account the roughness and terrain topography in which the contamination source is located. A two-dimensional pollution spreading model was constructed at the earth's surface level. In the papers (Olivera et al. 2013; Sanín and Montero 2007; Grazia et al. 2017; Kho et al. 2007; Walvekar and Gurjar 2013), a “box model” was constructed, which takes into account the wind direction and terrain relief. The emission substance SO₂ was considered and was used the *k*–epsilon turbulence model.

To simulate the spread of contamination from two chimneys of Ekibastuz SDPP-1, several test problems were first considered and solved numerically. This procedure is carried out in order to validate the numerical algorithm and the mathematical model. In the first test problem, a two-dimensional problem was examined. The obtained computational values were compared with the results from Schonauer and Adolph 2005 and Falconi et al. 2007, and good matches were obtained. In the second test problem, a three-dimensional jet in crossflow problem was examined. The obtained results were validated and compared with the numerical values from the paper (Keimasi and Taeibi-Rahni 2001), and measured values (Ajersch et al. 1995) showed a more accurate matching with the measured values than the data from computation (Keimasi and Taeibi-Rahni 2001). After solving the 2D and 3D test problems and validating the numerical algorithm, the distribution of atmospheric pollution from the Ekibastuz SDPP-1 was considered.

Ekibastuz SDPP-1 (Fig. 1) is the largest TPP in the Republic of Kazakhstan which is located in Ekibastuz city, which is between the Pavlodar and Semey cities. The design capacity of TPP is 4000 MW, and the working capacity is about 3500 MW. The Ekibastuz SDPP-1 is located on the northern shore of Zhyngyldy Lake, at 16 km north from the Ekibastuz city. The building dimensions: height—64 m, width—132 m and length—500 m. This TPP has two chimneys with heights are 300 m (built in 1980) and 330 m (built in 1982).





Fig. 1 Satellite image of the TPP and the distance between the two chimneys [250 (m)]. Ekibastuz SDPP-1, Ekibastuz city, Republic of Kazakhstan

Two-dimensional test problems

Scheme and dimensions of the computational domain

Figure 2 illustrates the scheme and the computational area dimensions. Substance A enters through the left side (inlet 1), substance B across the pipe input (inlet 2) and the output is on the right side (outlet). All computational domain size is indicated in Fig. 2.

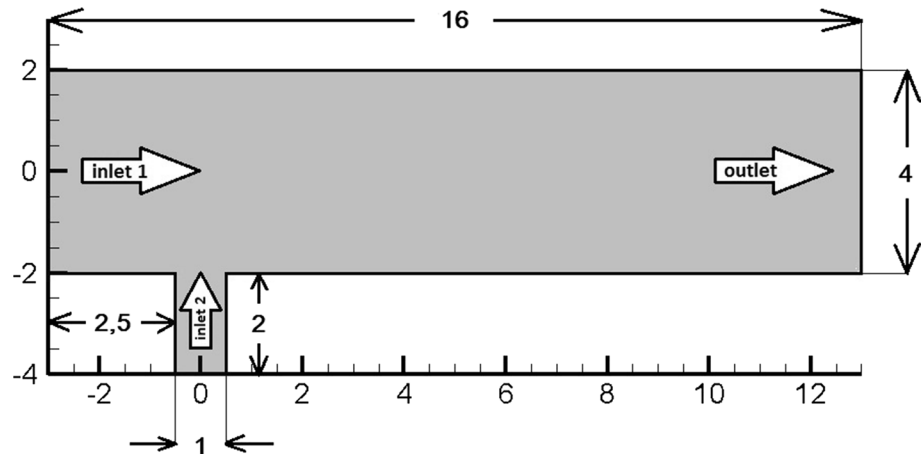
Materials and methods

Mathematical model

A detailed description of recent works devoted to the study of the contamination flow from a pipe in a transverse flow can be found in Su and Mungal (2004), Shan and Dimotakis (2006), Hasselbrink and Mungal (2001), Muppidi and

Mahesh (2005, 2007, 2008), Chochua et al. (2000), Acharya et al. (2001), Camussi et al. (2002), Schluter and Schonfeld (2000), Chai et al. (2015), Livescu et al. (2000). In paper (Kelso et al. 1996), the authors numerically modeled the velocity field, while in papers (Su and Mungal 2004; Shan and Dimotakis 2006) the passive scalar mass fraction field was considered. For solving such problems are almost always used numerical simulations. In papers (Hasselbrink and Mungal 2001; Muppidi and Mahesh 2008), Reynolds-averaged Navier–Stokes equations (RANS) were applied and the data were matched with the measured data. In papers (Chochua et al. 2000; Acharya et al. 2001; Camussi et al. 2002), a more accurate correspondence between numerical results was obtained by using the direct numerical simulation (DNS) method and real measurements. These problems were also examined in many papers (Schluter and Schonfeld 2000; Chai et al. 2015; Livescu et al. 2000). However, the direct numerical simulation method claims high computational costs, which is expensive for simulating the problems in actual sizes. That is why in this paper the k - ϵ

Fig. 2 Scheme and dimensions of the computational domain



turbulent model was used. The main equations representing these processes are the Navier–Stokes equations (Ferziger and Peric 2013; Issakhov et al. 2018, 2019; Issakhov and Mashenkova 2019), which consist of the continuity and momentum equations:

$$\frac{\partial u_j}{\partial x_j} = 0 \quad (1)$$

$$\frac{\partial \rho u_i}{\partial t} + \frac{\partial}{\partial x_j} (\rho u_i u_j) = -\frac{\partial p'}{\partial x_i} + \frac{\partial}{\partial x_j} \left[\mu_{\text{eff}} \left(\frac{\partial u_i}{\partial x_j} + \frac{\partial u_j}{\partial x_i} \right) \right] - \rho \tilde{g} \hat{n} \quad (2)$$

where μ_{eff} —the effective viscosity, p' —the modified pressure. Here $p' = p + 2\rho k/3 + 2\mu_{\text{eff}}/3 \partial u_k / \partial x_k$ and $\mu_{\text{eff}} = \mu + \mu_t$, where $\mu_t = C_\mu \rho k^2 / \varepsilon$ —the turbulence viscosity, p —the pressure, g —the gravity force, ρ —the density, u_j —the velocity components, \hat{n} —the normal vector. In order to close this equation system, a $k - \varepsilon$ turbulent model was used

$$\frac{\partial k}{\partial t} + \frac{\partial}{\partial x_j} (u_j k) = \frac{\partial}{\partial x_j} \left[\left(\mu + \frac{\mu_t}{\sigma_k} \right) \frac{\partial k}{\partial x_j} \right] + P_k - \rho \varepsilon + P_{kb} \quad (3)$$

$$\frac{\partial \varepsilon}{\partial t} + \frac{\partial}{\partial x_j} (u_j \varepsilon) = \frac{\partial}{\partial x_j} \left[\left(\mu + \frac{\mu_t}{\sigma_\varepsilon} \right) \frac{\partial \varepsilon}{\partial x_j} \right] + \frac{\varepsilon}{k} (C_{\varepsilon 1} P_k - C_{\varepsilon 2} \rho \varepsilon + C_{\varepsilon 1} P_{\varepsilon b}) \quad (4)$$

P_k —turbulence production due to viscous forces, which is presented as: $P_k = \mu_t \left(\frac{\partial u_i}{\partial x_j} + \frac{\partial u_j}{\partial x_i} \right) \frac{\partial u_i}{\partial x_j} - \frac{2}{3} \frac{\partial u_k}{\partial x_k} \left(3\mu_t \frac{\partial u_k}{\partial x_k} + \rho k \right)$, where P_{kb} , $P_{\varepsilon b}$ —the buoyancy forces, where $P_{kb} = -\frac{\mu_t}{\rho \beta} \rho \beta g_i \frac{\partial T}{\partial x_i}$ and $P_{\varepsilon b} = C_3 \max(0, P_{kb})$. β is the coefficient of thermal expansion, $\sigma_\rho = 0.9$, $C_\mu = 0.09$, $C_{\varepsilon 1}$, $C_{\varepsilon 2}$, σ_k , σ_ε —are constants.

To solve the species transport equations, ANSYS Fluent computes the local mass fraction of each species Y_i , by

the solution of a convection diffusion equation for the i th species.

$$\frac{\partial}{\partial t} (\rho Y_i) + \nabla \cdot (\rho \vec{u} Y_i) = -\nabla \cdot \vec{J}_i + R_i + S_i \quad (5)$$

where S_i is the rate of creation by addition from the dispersed phase plus any user-defined sources and R_i is the net rate of i species production by chemical reaction.

For the turbulent flows, the mass diffusion is computed as:

$$\vec{J}_i = -\left(\rho D_{i,m} + \frac{\mu_t}{Sc_t} \right) \nabla Y_i \quad (6)$$

where $Sc_t = \mu_t / \rho D_i$ —turbulent Schmidt number (D_i —the turbulent diffusivity and μ_t —the turbulent viscosity). The default Sc_t is 0.7. In this work, it was defined as 1.

The energy equation is computed as:

$$\frac{\partial}{\partial T} (\rho E) + \nabla \cdot (\vec{v} (\rho E + p)) = \nabla \cdot \left(k_{\text{eff}} \nabla T - \sum_j h_j \vec{J}_j + (\vec{\tau}_{\text{eff}} \cdot \vec{v}) \right) + S_h \quad (7)$$

where \vec{J}_j —the diffusion flux of species j , $k_{\text{eff}} = k + k_t$ —the effective conductivity, k_t —the turbulent thermal conductivity, set according to the turbulence model. The first three components on the RHS of (7) express energy transfer due to conduction, species diffusion and viscous dissipation, respectively. S_h take into account the chemical reaction energy, $E = h - \frac{p}{\rho} + \frac{v^2}{2}$, here $h = \sum_j Y_j h_j + \frac{p}{\rho}$, Y_j is the mass fraction of species j , $h_j = \int_{T_{\text{ref}}}^T c_{p,j} dT$, where $T_{\text{ref}} = 298.15$ K.

Mesh

There are a lot of different studies concerning the choice of optimal grid size. For instance, in the papers (Schonauer and Adolph 2005; Falconi et al. 2007) a computational result



analysis for three different grids is carried out. According to these data, the main part of the channel grid had 2561×641 dimensions; the pipe grid had 161×321 dimensions. As a result, the total number of elements was 1,693,121.

For the numerical simulations, which carried out at ANSYS Fluent, all values were set in meters; geometry was built in ANSYS Geometry. The grid for simulations by the TFS-MCM software has been built by using the Pointwise program. Details on the grid generation process and further details and application to various flow problems can be found in Issakhov (2014, 2015a, b, 2016a, b; 2017a, b). For the numerical algorithm was chosen the SIMPLE algorithm. Convergence condition was set as $\epsilon = 0.00001$. For numerical solving the distribution of the species mass fraction in the ANSYS Fluent, the species transport option was used.

Inlet conditions for the main pipe and the crossflow velocity are described by the different profiles. The velocity ratio is expressed through ratio $R = U_{jet}/U_{crossflow} = 1.5$. The results of different velocity profiles and their influence on the substances movement were compared. Substance B, outgoing from the pipe, reacts with the main flow substance A, thereby forming C. There each mass fraction of them has been studied. The species mass fraction is the species mass per unit of the mixture mass (e.g., kg of species in 1 kg of the mixture). The substances are selected for the purpose that the Damköhler number was 1. The flow was presented as incompressible due to the small Mach number and weak wind velocity. A similar study was conducted by the papers (Schonauer and Adolph 2005; Falconi et al. 2007), and the aim of this study was to compare the obtained numerical data with the previous results.

Boundary conditions

Boundary conditions were defined as follows: for the walls—“Wall,” for the outlet—“Pressure outlet,” for inlet 1 and inlet 2—“Velocity inlet.”

For the main channel input (inlet 1) were considered the different velocity profile u types (where u is the horizontal velocity component):

$$u1 : u = u^* \tag{8}$$

$$u2 : u = u^* \left(1 - e^{-4.5 \left(1 - \frac{r^2}{4} \right)} \right), \quad r = y \tag{9}$$

$$u3 : u = u^* \left(1 - e^{-5 \left(1 - \frac{r^2}{4} \right)} \right), \quad r = y \tag{10}$$

$$u4 : u = u^* \left(1 - e^{-5.5 \left(1 - \frac{r^2}{4} \right)} \right), \quad r = y \tag{11}$$

Other parameters were defined as constant: $w = 0$ (vertical velocity component), $Y_A = 1, Y_B = 0$.

For the pipe inlet (inlet 2): $Y_A = 0, Y_B = 1$;

$$u = 0, w = 2R u^* (1 - 4l^2), \quad l = x \tag{12}$$

where u^* changes depending on the selected material. In this case for substances A and B was set the oxygen O_2 . To obtain the necessary Reynolds number $Re = \frac{\rho u_{crossflow} D}{\mu} = 25$ and taking into account the fact that the dynamic viscosity of the oxygen is $\mu = 1.919e - 05 \text{ kg m}^2/\text{s}$, the density $\rho = 1.299874 \text{ kg/m}^3$, the velocity was determined as $u^* = 0.000369074233 \text{ m/s}$, temperature considered constant and the value set as $T = 300 \text{ K}$. The pipe diameter was $D = 1 \text{ m}$. In order to get the Schmidt number equal to 1, the diffusion coefficient was defined as the $0.677 \text{ m}^2/\text{s}$.

In the ANSYS Fluent, all simulations are made in real size, so the actual parameters have been specified in the present case. In the simulations by the TFS-MCM (Issakhov 2014, 2015a, b, 2016a, b, 2017a, b) were used dimensionless parameters. The boundary conditions are given in Table 1.

Results and discussion

Numerical results

Next, the numerical computational values and comparative analysis of the following parameters are presented: the velocity, mass fraction and temperature fields.

Velocity

Figure 3a–d) shows the results for the horizontal and vertical velocity profiles at the initial velocity profile $u3$ for the main channel. Below there are the velocity profiles u for different initial velocities at different distances $x/D = 0.0, x/D = 1.5, x/D = 3.0, x/D = 4.5$. Furthermore, Fig. 3e–h clearly shows that the difference between the profiles $u2, u3$ and $u4$ approximately similar, but the profile $u1$ is different from others. These results show that it is significant to define the velocity profile as a function, rather than uniform, since it greatly influences the value and more accurately describes the real physical processes.

Table 1 Boundary conditions

Parameters	Inlet 1	Inlet 2	Wall	Outlet
u	See (8)–(11)	$u=0$	$u=0$	$\frac{\partial u}{\partial x} = 0$
w	$w=0$	See (12)	$w=0$	$\frac{\partial w}{\partial x} = 0$
p	Equation (2)	$p=p_{atmosphere}$	Equation (2)	Equation (2)
Y_A	$Y_A=1$	$Y_A=0$	$\frac{\partial Y_A}{\partial x} = 0$	$\frac{\partial Y_A}{\partial x} = 0$
Y_B	$Y_B=0$	$Y_B=1$	$\frac{\partial Y_B}{\partial x} = 0$	$\frac{\partial Y_B}{\partial x} = 0$
Y_C	$Y_C=0$	$Y_C=0$	$\frac{\partial Y_C}{\partial x} = 0$	$\frac{\partial Y_C}{\partial x} = 0$

Fig. 3 Profiles of vertical and horizontal velocity components (m/s): **a** $x/D=0.0$, **b** $x/D=1.5$, **c** $x/D=3.0$, **d** $x/D=4.5$; and comparison of velocity profiles at different distances: **e** $x/D=0.0$, **f** $x/D=1.5$, **g** $x/D=3.0$, **h** $x/D=4.5$

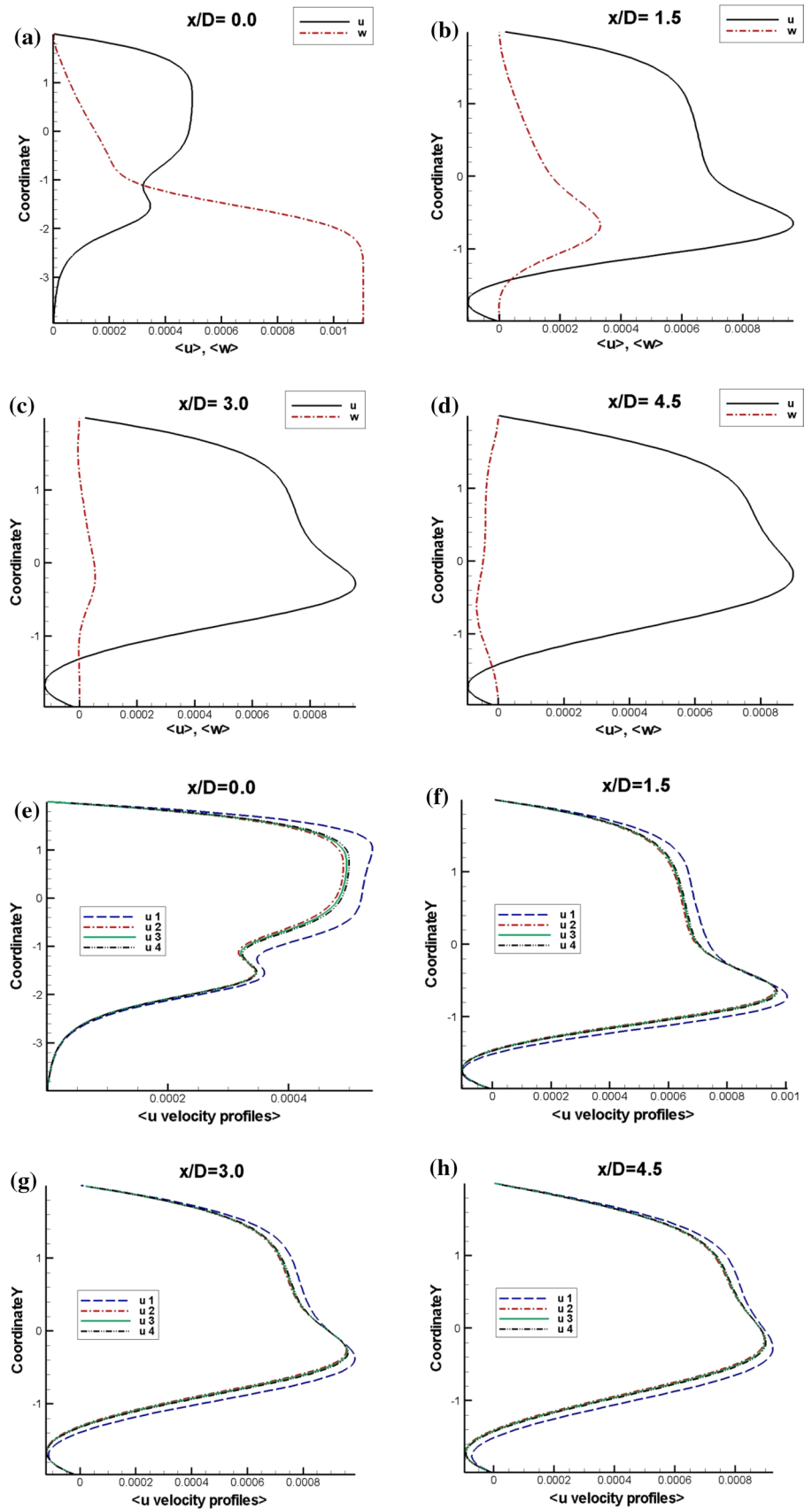


Figure 4a–c shows the flow streamlines and velocity magnitude values throughout the computational domain. Moreover, Fig. 4d–i illustrates the contours of u and w velocity components, respectively.

Differences in the numerical results are explained by the fact that physical values are specified in ANSYS, and dimensionless values are set in TFS-MCM. The obtained numerical results for velocity magnitude, horizontal velocity components and vertical velocity components were compared with numerical results from papers (Schonauer and Adolph 2005; Falconi et al. 2007). While Figure 4a, d, g shows the results from the paper (Schonauer and Adolph 2005; Falconi et al. 2007), in Fig. 4b, e, h, numerical results can be found obtained with the TFS-MCM, whereas Fig. 4c, f, i describes the numerical results obtained with the ANSYS Fluent.

Mass fraction

Figure 5a–l illustrates the mass fraction profile results of substances A, B and the resulting reactant C at different sections ($x/D = 0.0$, $x/D = 1.5$, $x/D = 3.0$, $x/D = 4.5$), respectively. They also clearly show that the difference between the velocity profile $u1$ and others has the influence to the species mass fraction distributions too.

Figure 6a–i illustrates a comparative analysis of the mass fractions spread obtained in this work by TFS-MCM and ANSYS with the results obtained from papers

(Schonauer and Adolph 2005; Falconi et al. 2007), where C1, C2 and C3—the mass fraction of substances A, B and C, respectively.

Figure 6j, k shows the temperature distribution results obtained by performing calculations on the TFS-MCM and ANSYS.

The three-dimensional test problem

The computational domain

The simulation region of the test problem is a three-dimensional channel with the pipe entering into it. The transverse channel length is $45D$, the width is $3D$, the pipe center is located at $5D$ from the inlet, the crossflow channel height is $20D$, and the pipe height is $5D$ (Fig. 7).

Characteristics of the flow

The flow velocity ratio from the pipe to the vertical flow velocity is marked by R and is calculated as follows:

$$R = V_{\text{jet}}/V_{\text{crossflow}} \quad (13)$$

In the study (Keimasi and Taeibi-Rahni 2001), different R s (0.5, 1.0 and 1.5) were studied. The crossflow pipe velocity was 5.5 m/s. In this work, the ratio $R = 0.5$ was tested, so the flow velocity in the vertical flow was defined

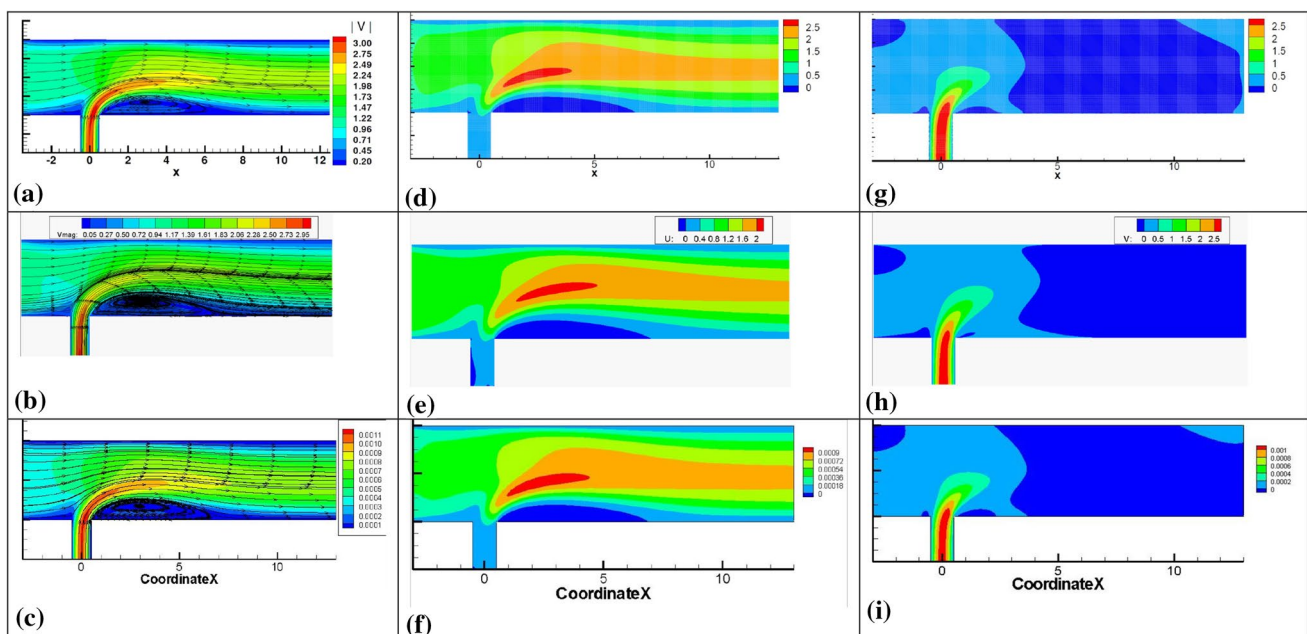


Fig. 4 Contour of velocity magnitude and streamlines: **a** results of (Schonauer and Adolph 2005; Falconi et al. 2007), **b** results obtained by calculations on TFS-MCM software, **c** results obtained by ANSYS. Contour of the u velocity component: **d** results of (Schonauer and Adolph 2005; Falconi et al. 2007), **e** results obtained by

calculations on TFS-MCM software; **f** results obtained by ANSYS. The contour of the w velocity component: **g** results of (Schonauer and Adolph 2005; Falconi et al. 2007), **h** results obtained by calculations on TFS-MCM software, **i** results obtained by ANSYS

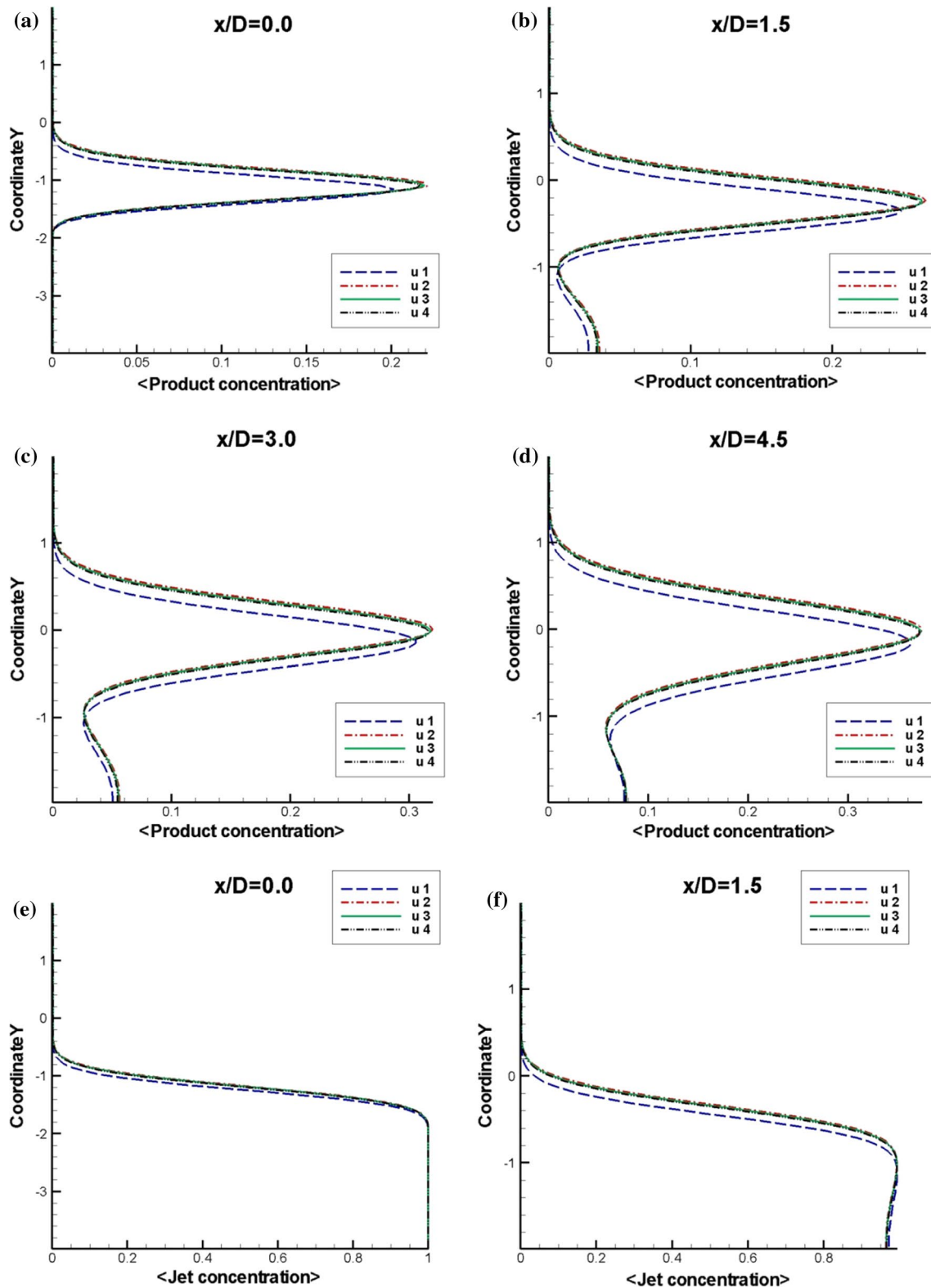


Fig. 5 Profiles of mass fraction for the reaction product C at different distances for various initial velocity profiles: **a** $x/D=0.0$, **b** $x/D=1.5$, **c** $x/D=3.0$, **d** $x/D=4.5$. Profiles of substance B mass fraction at different distances for various initial velocity profiles: **e** $x/D=0.0$, **f**

$x/D=1.5$, **g** $x/D=3.0$, **h** $x/D=4.5$. Profiles of substance A mass fraction at different distances for various initial velocity profiles: **i** $x/D=0.0$, **j** $x/D=1.5$, **k** $x/D=3.0$, **l** $x/D=4.5$



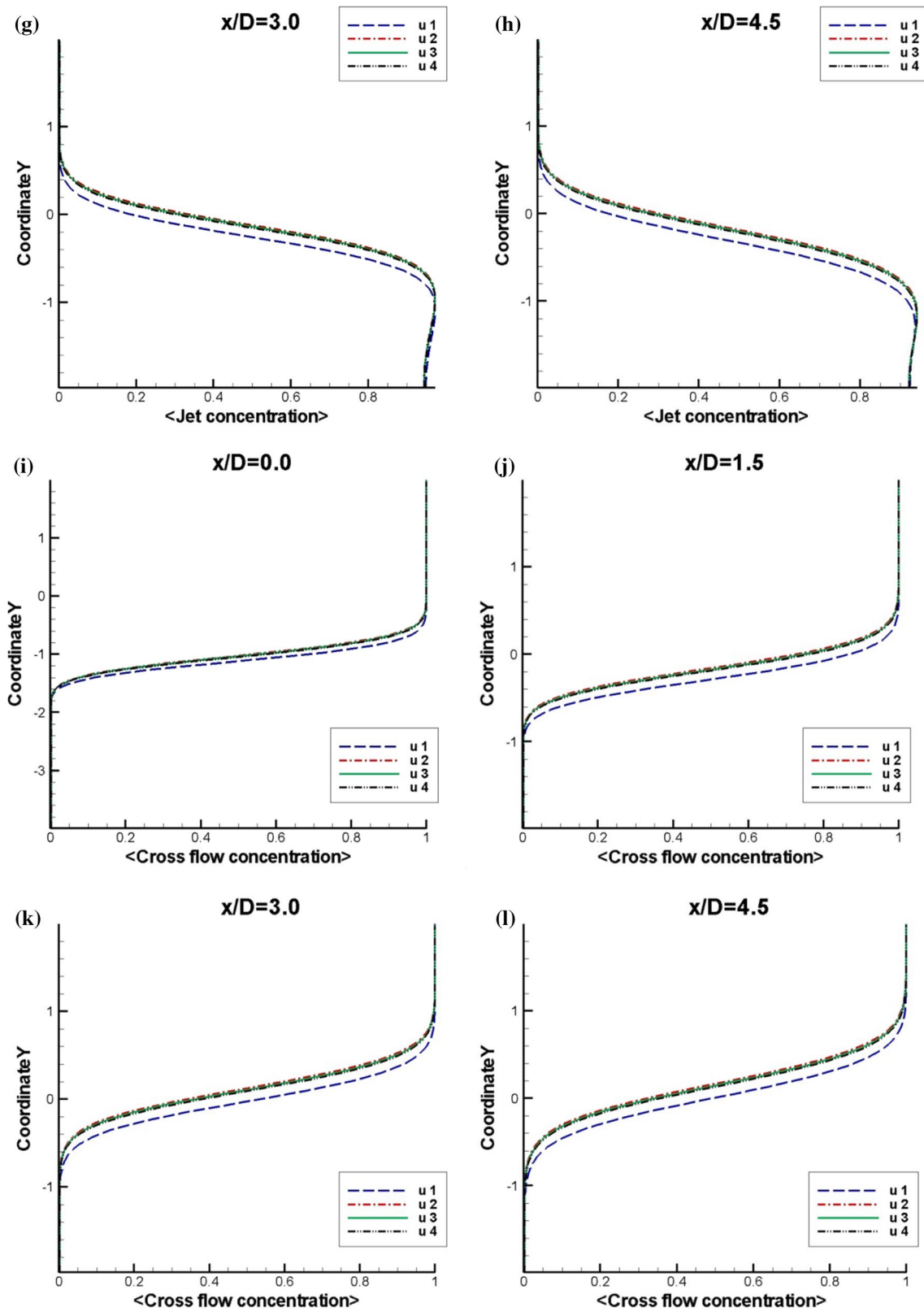


Fig. 5 (continued)

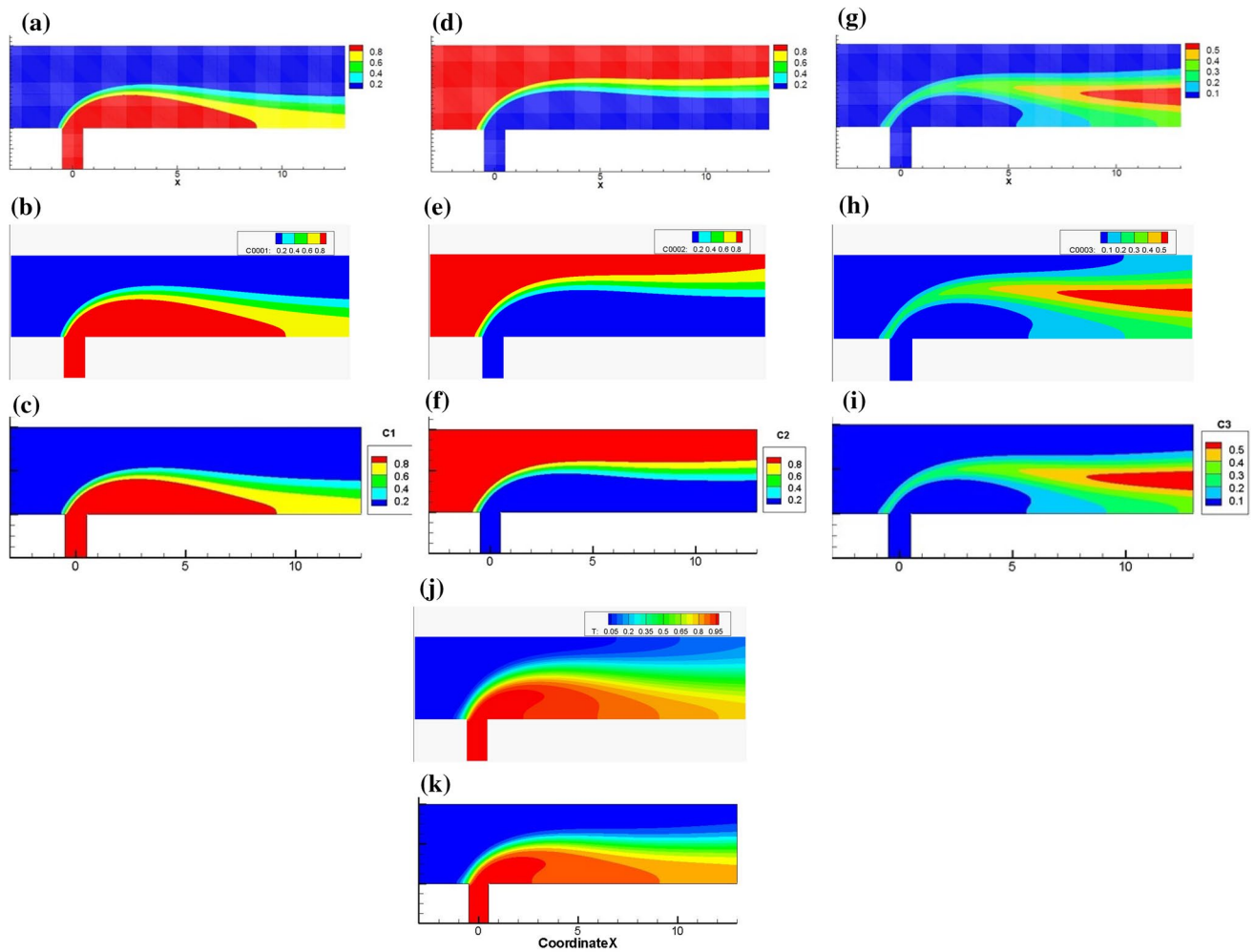


Fig. 6 Comparative analysis of the substance A distribution: **a** results of Schonauer and Adolph (2005, Falconi et al. (2007), **b** results obtained by calculations on TFS-MCM software; **c** results obtained by ANSYS. Comparative analysis of the substance B distribution: **d** results of Schonauer and Adolph (2005), Falconi et al. (2007), **e** results obtained by calculations on TFS-MCM software; **f** results

obtained by ANSYS. Comparative analysis of the substance C distribution: **g** results of Schonauer and Adolph (2005), Falconi et al. (2007), **h** results obtained by calculations on TFS-MCM software; **i** results obtained by ANSYS. Comparative analysis of the temperature field: **j** results obtained by calculations on TFS-MCM software; **k** results obtained by ANSYS

as 11 m/s. The pipe diameter was $D = 12.7$ mm. On the basis of the considering velocity, the Reynolds number was $Re_{jet} = \rho V_{jet} D / \mu = 4700$. The air was chosen as the substance material.

Boundary conditions

As shown in Fig. 7, the following boundary condition types were used for solving the problem: inlet, wall, outlet, periodic, no flux. Based on the measured value, the boundary layer width is $2D$. To characterize the initial transverse velocity profile in the boundary layer was used $1/7$ power law wind profile.

$$\frac{u}{u_r} = \left(\frac{z}{z_r} \right)^\alpha \quad (14)$$

where α is an empirically derived coefficient that varies due to the atmosphere stability and u_r is the known wind velocity at a reference height z_r , and u is the wind velocity at height z . The neutral stability conditions are given as $\alpha = 1/7$. Above the boundary layer, the velocity is defined as a uniform (11 m/s) (Keimasi and Taeb-Rahni 2001).

The obtained numerical results

In this work, the case $R=0.5$ was studied. Figure 8 illustrates the matching of values for the lateral velocity component at jet center plane ($z/D=0$) for $R=0.5$ with the measured values (Keimasi and Taeb-Rahni 2001) and the experimental values (Ajersch et al. 1995) for the cross section $x/D=3$ and $x/D=0$. The results of present work are marked by the red solid line, round-shaped measured values (Ajersch et al.



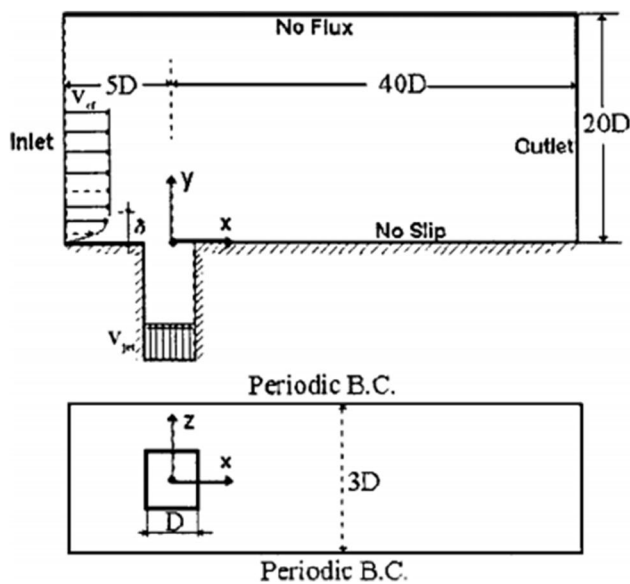


Fig. 7 Computational domain parameters

1995), and the rest illustrates the obtained numerical data (Keimasi and Taeibi-Rahni 2001) by using various turbulent models. Also, the values obtained by using the SST $k - \omega$ turbulent model are illustrated. From these figures, it can be seen that the selected $k - \epsilon$ model and SIMPLE method allow obtaining the values closest to the experimental results.

So it can be observed from the figures that the computational values of the horizontal and vertical velocity components describe the motion character well in comparison with the measured values (Ajersch et al. 1995). These results can be explained by the fact that for a given numerical simulation the finer computational grid was used, which clustered near the wall than for simulation in the work (Keimasi and Taeibi-Rahni 2001).

The three-dimensional problem in real physical scale

In this section, a three-dimensional problem in actual physical size is considered. The comparative analysis was carried out with work (Zavila 2012). The results of Zavila 2012 were checked by a measured performed in a low-speed wind tunnel.

Computational area and mesh

The three-dimensional box with a chimney was selected as the computational area. The emissions are emitted from the chimney hole. Figure 9a, b illustrates the geometry and computational mesh. The dimensions are represented in

Table 2. For precise modeling, the computational mesh was non-uniform and was clustered close to the ground, near the chimney outlet and approximately along the pollution motion trajectory. The total number of three-dimensional element number is 568,486. Furthermore, it should be noted that according to Chang et al. 2011 and Saeed et al. 2017, the RNG $k - \epsilon$ and the standard $k - \epsilon$ models give nearly the equal values for the similar problem. So, the test problem was simulated using the Standard $k - \epsilon$ model, but in this work RNG $k - \epsilon$ model was used. It was done in order to match the obtained values with results of Zavila (2012).

The boundary conditions and comparison of obtained numerical results

Boundary conditions were defined as the “Wall” for chimney walls and the ground, “Velocity inlet” for the wind inlet and the chimney hole, “Symmetry” for the side walls and the top wall and “Pressure Outlet” for the outlet.

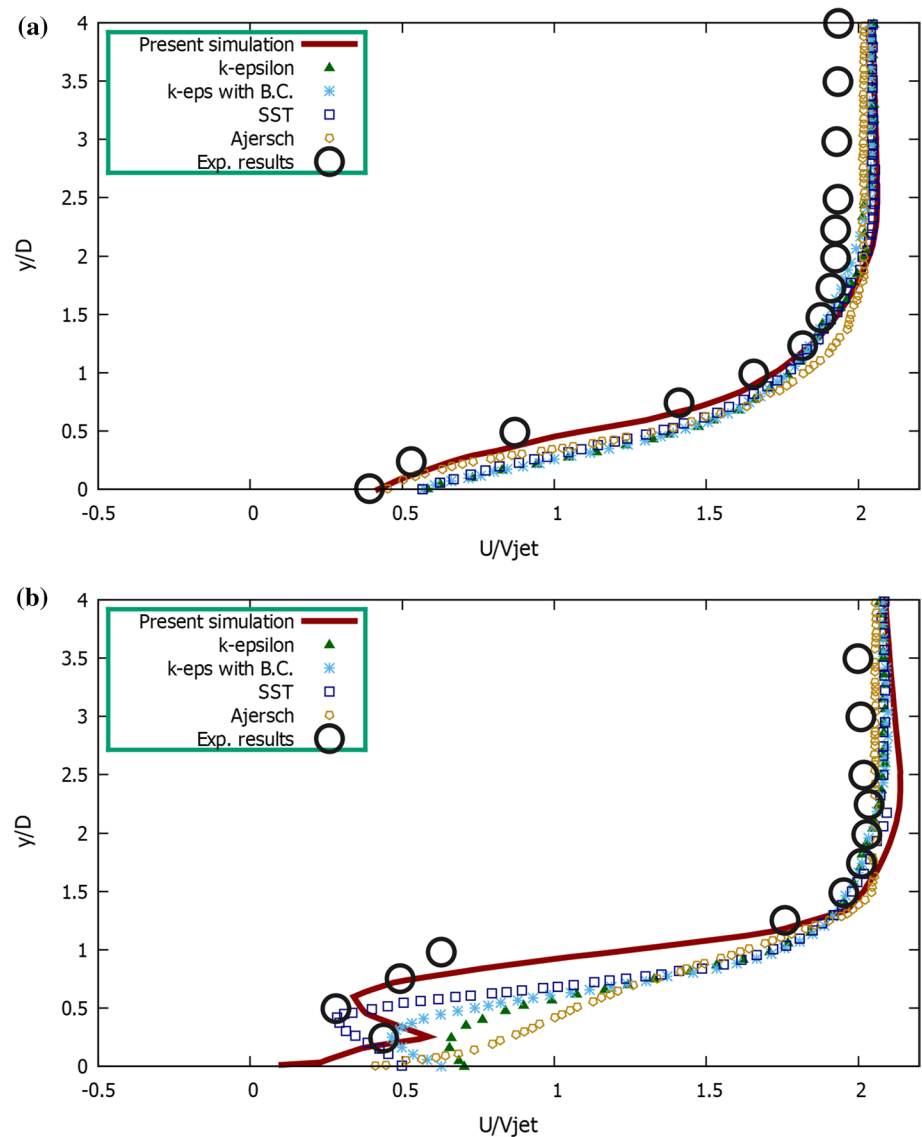
In the paper (Zavila 2012), the author assumed the He dispersion for various wind velocities: 1, 3 and 5 m/s. For matching with the paper, it was selected the third case ($v_{\text{air}} = 5$ m/s) (see Fig. 9c). In the test problem for species movement simulation was used species transport model. It was considered that discharged concentration do not react with air. The gravitational force impact was taken into account. The convergence criterion and temperature were defined as $\epsilon = 0.0001$ and 300 K, respectively. All characteristics were specified similar to Zavila (2012).

Figure 9d illustrates good correspondence with the numerical values (see Fig. 9c) (Zavila 2012). The numerical values were illustrated as pollutant concentrations iso-surfaces and the high mass fraction value was defined as 0.00003.

The Ekibastuz SDPP-1

Next, the pollution distribution of the real physical model for the Ekibastuz SDPP-1, in the Ekibastuz city, was considered. The Ekibastuz SDPP-1 species emits from two chimneys with heights 330 m and 300 m. The space between the two chimneys is about 250 m (see Fig. 1). The chimneys diameters were set as 10 m. For simulation were considered two cases with various wind velocities: 1.0 m/s and 1.5 m/s (Fig. 10a, b). The pollutant emission velocity from chimneys is 5 m/s. In order to characterize the boundary layer, the following wind velocity profile was set $v_x = v_{\text{wind}} \cdot (0.2371 \cdot \ln(Y + 0.00327) + 1.3571)$ (m/s). In this case, the CO_2 was defined as a pollutant (see Fig. 10a, b). Figure 10a, b shows that at strong wind velocity drops down the pollution on the ground surface much farther from the source than at weak wind velocities. Further, height

Fig. 8 Comparison of the lateral velocity component values at jet center plane ($z/D=0$) for $R=0.5$ with the numerical data (Keimasi and Taeibi-Rahni 2001) and the measured values (Ajersch et al. 1995): **a** $x/D=0$; **b** $x/D=3$



effect of the thermal power plant chimney was investigated. For this aim, mass fraction profiles from two chimneys were matched at various distances from the source [1750 and 2150 (m) (see Fig. 10c, d)] with wind velocity 1.5 m/s.

Figure 10a obviously illustrates that concentration from a lower chimney (300 m) drops down closer to the emission source. Figure 10c outlines comparison of CO_2 concentration profiles for a distance of 1750 m from the emission source. From the obtained numerical solutions, it can be noted that the discharged concentration from a small chimney (300 m) already reaches the land surface. And the level of concentration from a high chimney (330 m) is approximately equal to zero. However, when comparing values at an altitude of 150–350 m, it is observed that the released substance from the lower chimney (300 m) has a high value,

whereas for a high chimney (330 m) the concentration value has a lower value. This is due to the fact that in a given altitude range, the concentrations from the two chimneys are mixed because the space between the two chimneys is only 250 m, since the pollutions can dissipate well. From the obtained data, it can be noted that at a distance of 2150 m, the pollution from two chimneys is almost deposited on the land surface. It should be noted that the concentration (CO_2) value has higher values on the surface of the land than at a height (~ 300 m), since at this height the diffusion effect is insignificant. This phenomenon is connected with turbulent vortex dissipation. In paper (Toja-Silva et al. 2017), the authors illustrated that the species change trajectory and settle below toward the land at a distance approximately 500 m from the chimney. Nevertheless, despite that, at a distance of



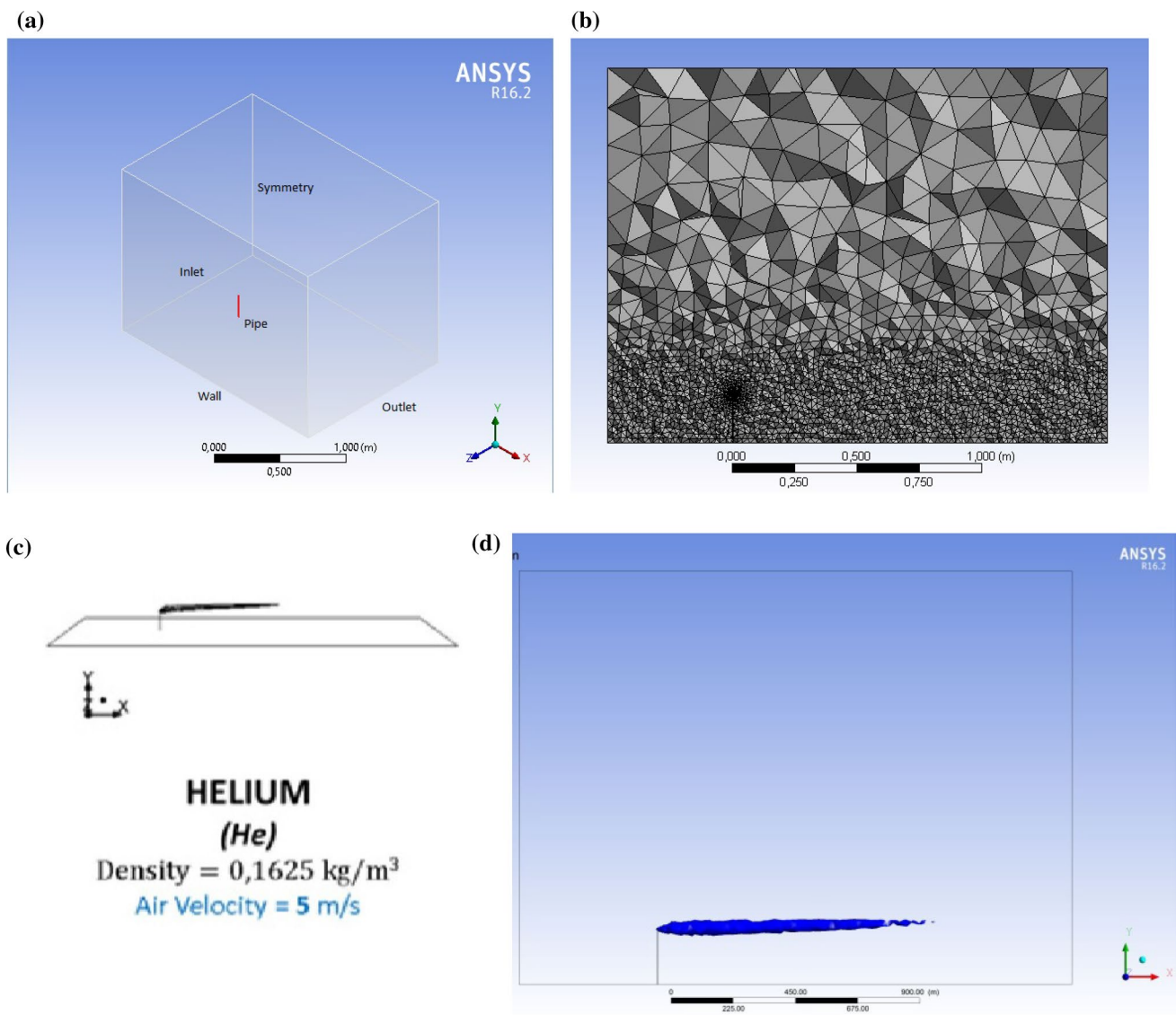


Fig. 9 Three-dimensional problem in actual physical size: **a** geometry of calculating domain; **b** unstructured grid. The He distribution values: data of Zavila (2012) (c) and present paper data (wind velocity is 5 m/s) (d)

Table 2 Geometry parameters

Geometry dimensions (m)	Stack dimensions (m)	Inlet dimensions (m)	Coordinates of stack (m)
1:1 X=2000 Y=1500 Z=1500	X=3.5 Y=200 Z=3.5	X=3.5 Y=3.5	X=500 Y=0.0 Z=750

approximately 700 m from the Ekibastuz SDPP-1, high concentration values can be noticed close to the ground level. However, this effect is also can be seen in the paper (Toja-Silva et al. 2017), but there are differences in the sedimentation distances due to different chimney heights.

Conclusion

The purpose of this work was to determine the distance at which the concentration from the chimney settles, and the factors affecting it, as well as the effect of the chimney height on the distribution of pollution. For this objective, a CFD modeling of dispersion and gaseous pollutant plume motion in real atmospheric conditions was conducted. The impact of different wind velocities and chimney heights was studied. To check the numerical algorithm and mathematical model, two test problems were simulated: two-dimensional and three-dimensional. The computational result of the three-dimensional test problems was compared with the measured data (Ajersch et al. 1995) and values from computation

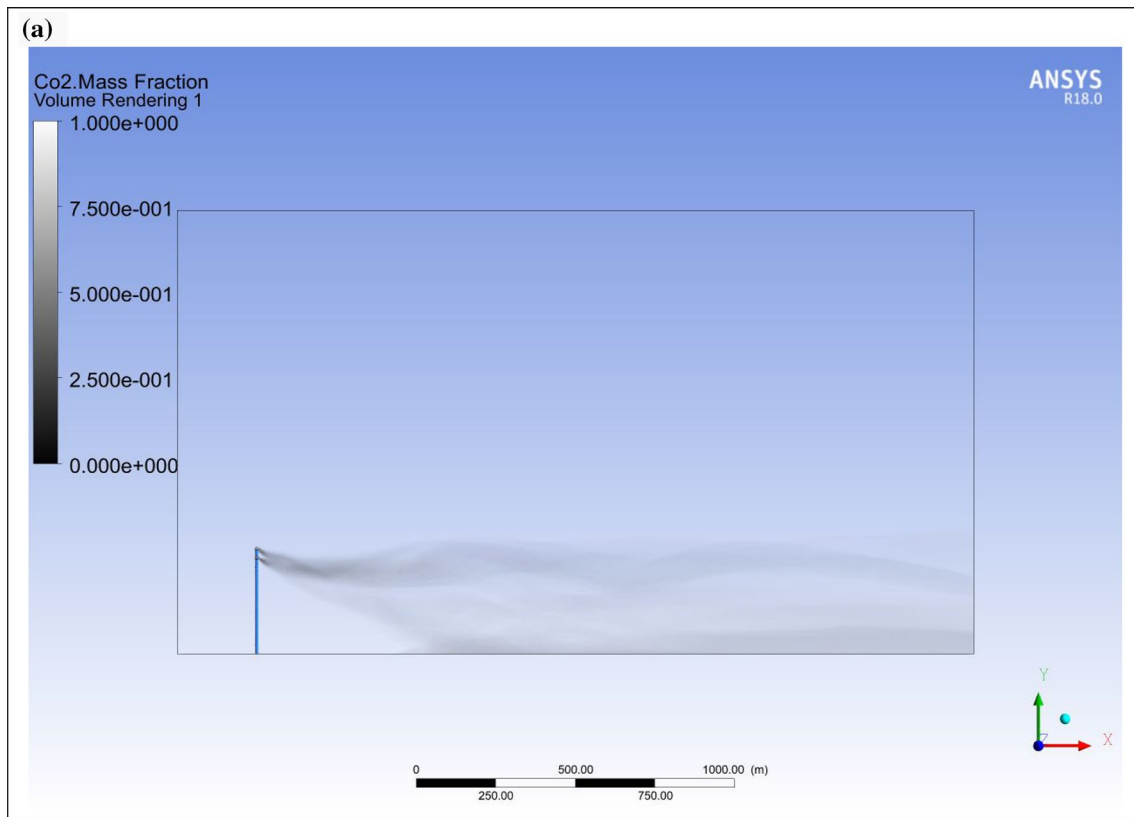


Fig. 10 Distribution of CO₂ from the thermal power for different wind velocities: **a** 1.0 m/s, **b** 1.5 m/s. Comparison of the CO₂ mass fraction profiles at different distances for two chimneys [330 and 300 (m)]: **c** 1750 (m), **d** 2150 (m). Wind velocity: 1.5 m/s

(Keimasi and Taeibi-Rahni 2001). The obtained values gave well agreement with the measured data. After proving the numerical algorithm and mathematical model, they were applied to the real-size problem. It should be noticed that numerical values in this paper were found to be almost the same as the measured values than numerical values obtained by other authors due to the improved computational mesh configuration and density. Next, a three-dimensional modeling of pollution spread in actual physical size was studied. Also the spread of the CO₂ was considered. The fine computational mesh was used close to the ground, near the chimney outlet and along the pollution motion trajectory.

Additionally the actual physical model of the pollution spread from Ekibastuz SDPP-1 (Ekibastuz city) was considered. The extraordinary feature of this TPP is that the pollution discharges from two chimneys with various heights (330

and 300 m). From the computational values, it is clear that the height of the chimneys essentially impacts the concentration spread. Obviously, the construction of higher chimneys leads to more corresponding for the ecology safety. Furthermore, future increases in computational power will be accompanied by claims of researchers for increased number of mesh elements and the inclusion of additional physical characteristics. Therefore, new treatments are needed in order to decrease modeling computational costs. The ecology safeness distances (2150 m for the second chimney (330 m) and 1750 for the first chimney (300 m)) were also specified the concentration drop down from the two chimneys of the thermal power plant.

Future investigation should proceed to investigate knowledge in describing the spread of harmful substances in the air at different distances. It would help to minimize the harm caused by emissions to people, fauna and flora and to define



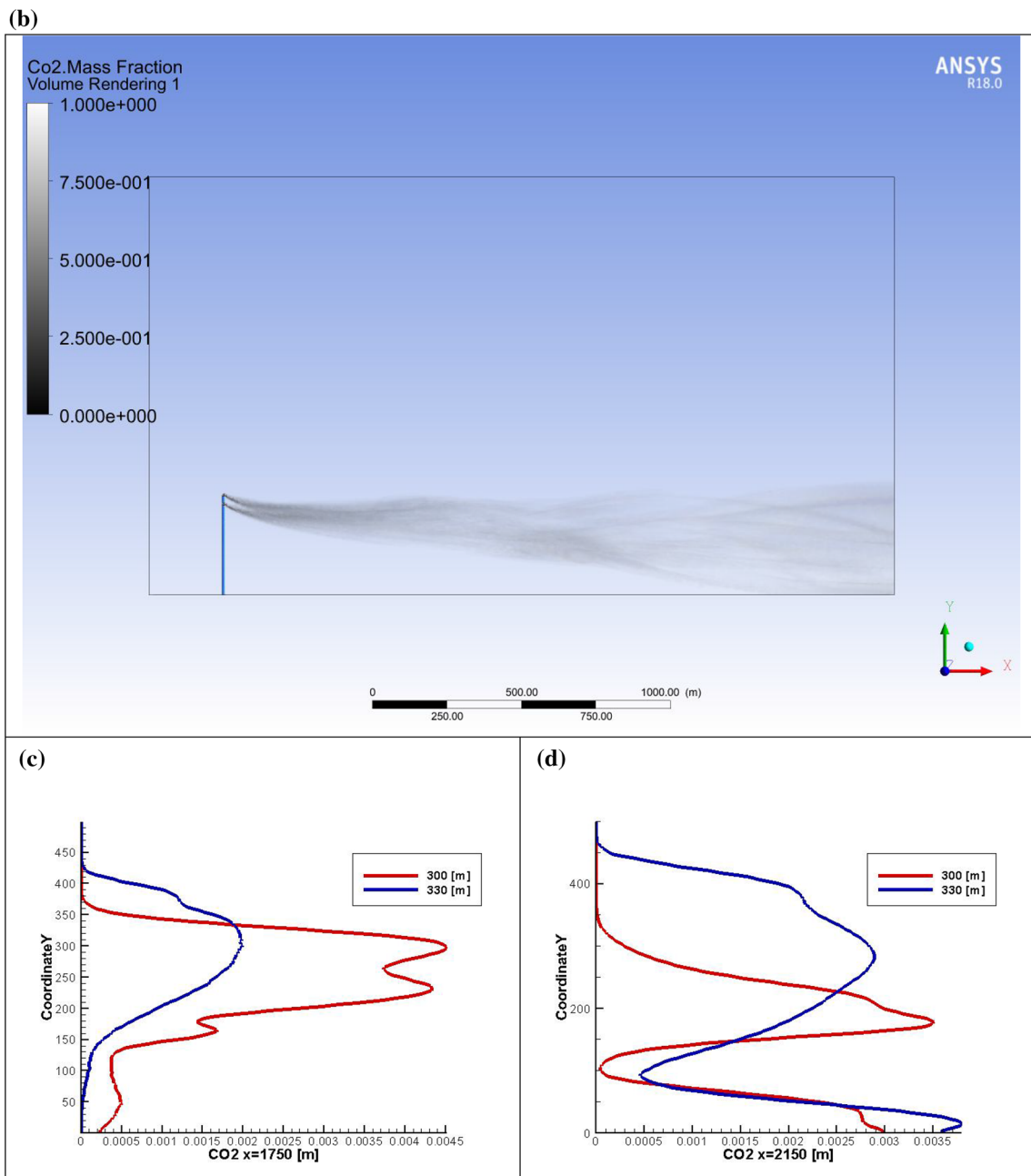


Fig. 10 (continued)

the optimal location of new TPPs with respect to cities or towns in advance.

It should be noticed that various limitations may exist in this study. The first limitation is the number of mesh elements: The lack of computer resources limited us in the mesh size. The second limitation is the complexity of implementing and analyzing measured researches at the Ekibastuz SDPP-1 (negligible differences between subjects, environmental factors and other unexpected changes during the experiment). These works are useful for those who are interested in gas pollutant spread in the environment.

Acknowledgements This work is supported by the grant from the Ministry of Education and Science of the Republic of Kazakhstan.

Compliance with ethical standards

Conflict of interest The authors declare that there is no conflict of interests regarding the publication of this paper.

References

- Abbaspour M, Javid AH, Moghimi P, Kayhan K (2005) Modeling of thermal pollution in coastal area and its economical and environmental assessment. *Int J Environ Sci Tech* 2(1):13–26
- Acharya S, Tyagi M, Hoda A (2001) Flow and heat transfer predictions for film-cooling. *Ann NY Acad Sci* 934:110–125
- Ajersch P, Zhou JM, Ketler S, Salcudean M, Gartshore IS (1995) Multiple jets in a crossflow: detailed measurements and numerical simulations. In: International gas turbine and aeroengine congress and exposition, ASME Paper 95-GT-9, Houston, TX, pp 1–16
- Annual report. SAMRYK ENERGY (2015) <https://www.samruk-energy.kz/en/shareholder/annual-reports>
- Barbero R, Cuadra D, Domingo J, Iranzo A, Gallego E (2015) Investigation of the near-range dispersion of particles unexpectedly released from a nuclear power plant using CFD. *Environ Fluid Mech* 15(1):67–83
- Camussi R, Guj G, Stella A (2002) Experimental study of a jet in a crossflow at very low Reynolds number. *J Fluid Mech* 454:113–144
- Chai X, Iyer PS, Mahesh K (2015) Numerical study of high speed jets in crossflow. *J Fluid Mech* 785:152–188
- Chang C-H, Chan C-C, Cheng K-J, Lin J-S (2011) Computational fluid dynamics simulation of air exhaust dispersion from negative isolation wards of hospitals. *Eng Appl Comput Fluid Mech* 5(2):276–285. <https://doi.org/10.1080/19942060.2011.11015370>
- Chochua G, Shyy W, Thakur S, Brankovic A, Lienau K, Porter L, Lischinsky D (2000) A computational and experimental investigation of turbulent jet and crossflow interaction. *Numer Heat Transf A* 38:557–572
- Ebrahimi M, Jahangirian A (2013) New analytical formulations for calculation of dispersion parameters of Gaussian model using parallel CFD. *Environ Fluid Mech* 13(2):125–144
- El-Sharkawi MA (2013) *Electric energy—an introduction*, 3rd edn. CRC Press, Boca Raton, p 53
- Environmental, Health, and Safety Guidelines for Thermal Power Plants. International Finance Corporation (2017). https://www.ifs.org/wps/wcm/connect/topics_ext_content/ifc_external_corporate_site/sustainability-atifc/policies-standards/ehs-guidelines
- Falconi CJ, Denev JA, Frohlich J, Bockhorn H (2007) A test case for microreactor flows—a two-dimensional jet in crossflow with chemical reaction. Internal report. available at: <http://www.ict.uni-karlsruhe.de/index.pl/themen/dns/index.html>: “2d test case for microreactor flows. Internal report. 2007 July 20
- Fatehifar E, Elkamel A, Alizadeh Osalu A, Charchi A (2008) Developing a new model for simulation of pollution dispersion from a network of stacks. *Appl Math Comput* 206:662–668
- Fay JA, Rosenzweig JJ (1980) An analytical diffusion model for long distance transport of air pollutants. *Atmos Environ* 14(3):355–365
- Ferziger JH, Peric M (2013) *Computational methods for fluid dynamics*, 3rd edn. Springer, Berlin, p 426
- Gousseau P, Blocken B, Stathopoulos T, Van Heijst GJF (2011) CFD simulation of near-field pollutant dispersion on a high-resolution grid: a case study by LES and RANS for a building group in downtown Montreal. *Atmos Environ* 45(2):428–438
- Grazia G, Sara F, Barbara A, Giorgio V, Alessandro B, Sergio T (2017) Impact assessment of pollutant emissions in the atmosphere from a power plant over a complex terrain and under unsteady winds. *Sustainability* 9:2076. <https://doi.org/10.3390/su9112076>
- Hasselbrink EF, Mungal MG (2001) Transverse jets and jet flames. Part 1. Scaling laws for strong transverse jets. *J Fluid Mech* 443:1–25
- Igbokwe JO, Azubuike JO, Nwufu OC, Okafor G, Ezurike BO, Opara UV (2016) Critical review and analysis of general pollutants associated with thermal power plants in Nigeria and control techniques. *Res Rev J Eng Technol* 5(4):1–4
- Issakhov A (2014) Modeling of synthetic turbulence generation in boundary layer by using zonal RANS/LES method. *Int J Non-linear Sci Numer Simul* 15(2):115–120. <https://doi.org/10.1515/ijnsns-2012-0029>



- Issakhov A (2015a) Mathematical modeling of the discharged heat water effect on the aquatic environment from thermal power plant. *Int J Nonlinear Sci Numer Simul* 16(5):229–238. <https://doi.org/10.1515/ijnsns-2015-0047>
- Issakhov A (2015b) Numerical modeling of the effect of discharged hot water on the aquatic environment from a thermal power plant. *Int J Energy Clean Environ* 16(1–4):23–28. <https://doi.org/10.1615/InterJEnerCleanEnv.2016015438>
- Issakhov A (2016a) Mathematical modeling of the discharged heat water effect on the aquatic environment from thermal power plant under various operational capacities. *Appl Math Model* 40(2):1082–1096. <https://doi.org/10.1016/j.apm.2015.06.024>
- Issakhov A (2016) Mathematical modelling of the thermal process in the aquatic environment with considering the hydro-meteorological condition at the reservoir-cooler by using parallel technologies. In: *Sustaining power resources through energy optimization and engineering*, pp 1–494. <https://doi.org/10.4018/978-1-4666-9755-3> Chapter 10, pp 227–243. <https://doi.org/10.4018/978-1-4666-9755-3.ch010>
- Issakhov A (2017a) Numerical study of the discharged heat water effect on the aquatic environment from thermal power plant by using two water discharged pipes. *Int J Nonlinear Sci Numer Simul* 18(6):469–483. <https://doi.org/10.1515/ijnsns-2016-0011>
- Issakhov A (2017) Numerical modelling of the thermal effects on the aquatic environment from the thermal power plant by using two water discharge pipes. In: *AIP conference proceedings*, vol 1863, p 560050. <http://dx.doi.org/10.1063/1.4992733>
- Issakhov A, Mashenkova A (2019) Numerical study for the assessment of pollutant dispersion from a thermal power plant under the different temperature regimes. *Int J Environ Sci Technol*. <https://doi.org/10.1007/s13762-019-02211-y>
- Issakhov A, Zhandaulet Y, Nogaeva A (2018) Numerical simulation of dam break flow for various forms of the obstacle by VOF method. *Int J Multiph Flow* 109:191–206
- Issakhov A, Bulgakov R, Zhandaulet Y (2019) Numerical simulation of the dynamics of particle motion with different sizes. *Eng Appl Comput Fluid Mech* 13(1):1–25
- Keimasi MR, Taeibi-Rahni M (2001) Numerical simulation of jets in a crossflow using different turbulence models. *AIAA J* 39(12):2268
- Kelso RM, Lim TT, Perry AE (1996) An experimental study of round jets in cross-flow. *J Fluid Mech* 306:111–144
- Kho WLF, Sentian J, Radojevi M, Tan CL, Law PL, Halipah S (2007) Computer simulated versus observed NO₂ and SO₂ emitted from elevated point source complex. *Int J Environ Sci Technol* 4(2):215–222
- Kozic MS (2015) A numerical study for the assessment of pollutant dispersion from Kostolac b power plant to Viminacium for different atmospheric conditions. *Therm Sci* 19(2):425–434
- Livescu D, Jaber FA, Madnia CK (2000) Passive-scalar wake behind a line source in grid turbulence. *J Fluid Mech* 416:117–149
- Muppidi S, Mahesh K (2005) Study of trajectories of jets in crossflow using direct numerical simulations. *J Fluid Mech* 530:81–100
- Muppidi S, Mahesh K (2007) Direct numerical simulation of round turbulent jets in crossflow. *J Fluid Mech* 574:59–84
- Muppidi S, Mahesh K (2008) Direct numerical simulation of passive scalar transport in transverse jets. *J Fluid Mech* 598:335–360
- Olague EP, Knipping E, Shaw S, Ravindran S (2016) Microscale air quality impacts of distributed power generation facilities. *J Air Waste Manag Assoc*. <https://doi.org/10.1080/10962247.2016.1184194>
- Olivera A, Monterob G, Montenegro R, Rodriguez E, Escobar JM, Perez-Fogueta A (2013) Adaptive finite element simulation of stack pollutant emissions over complex terrains. *Exergy Int J* 49:47–60
- Saeed M, Yu J-Y, Abdalla AAA, Zhong X-P, Ghazanfar MA (2017) An assessment of k-ε turbulence models for gas distribution analysis. *Nucl Sci Tech* 28:146. <https://doi.org/10.1007/s41365-017-0304-x>
- Sanín N, Montero G (2007) A finite difference model for air pollution simulation. *Adv Eng Softw* 38:358–365
- Schluter JU, Schonfeld T (2000) LES of jets in crossflow and its application to a gas turbine burner. *Flow Turbul Combust* 65:177–203
- Schonauer W, Adolph T (2005) Results of the snuff problem Denev by the FDEM Program. Abschlussbericht des Verbundprojekts FDEM, Universität Karlsruhe
- Shan JW, Dimotakis PE (2006) Reynolds-number effects and anisotropy in transverse-jet mixing. *J Fluid Mech* 566:47–96
- Su LK, Mungal MG (2004) Simultaneous measurement of scalar and velocity field evolution in turbulent crossflowing jets. *J Fluid Mech* 513:1–45



- Toja-Silva F, Chen J, Hachinger S, Hase F (2017) CFD simulation of CO₂ dispersion from urban thermal power plant: analysis of turbulent Schmidt number and comparison with Gaussian plume model and measurements. *J Wind Eng Ind Aerodyn* 169:177–193
- Tomiyama H, Kobayashi S, Tanabe K, Chatani S, Takami A (2016) Temporal emission distribution corresponding to operating quantity in thermal power plant. *J Jpn Soc Atmos Environ* 51(2):124–131
- U.S. Environmental Protection Agency (2016) Clean Air Markets Division: <https://ampd.epa.gov/ampd/>
- Walvekar PP, Gurjar BR (2013) Formulation, application and evaluation of a stack emission model for coal-based power stations. *Int J Environ Sci Technol* 10(6):1235–1244
- WHO (2002) The world health report 2002—reducing risks, promoting healthy life. <http://www.who.int/whr/2002/en/>
- Zavila O (2012) Physical Modeling of gas pollutant motion in the atmosphere. *Adv Model Fluid Dyn*. Dr. Chaoqun Liu (Ed.), InTech. <https://doi.org/10.5772/48405>

